Applied Catalysis B: Environmental 165 (2015) 103–110

Contents lists available at ScienceDirect

Applied Catalysis B: Environmental

journal homepage: www.elsevier.com/locate/apcatb

In-situ fabrication of supported iron oxides from synthetic acid mine drainage: High catalytic activities and good stabilities towards electro-Fenton reaction

Min Sun*, Xiao-Rui Ru, Lin-Feng Zhai

Department of Chemical Engineering, Hefei University of Technology, Hefei, 230009, China

ARTICLE INFO

Article history:
Received 13 May 2014
Received in revised form 1 September 2014
Accepted 30 September 2014
Available online 8 October 2014

Keywords:
Air-cathode fuel cell
RhB degradation, Surface-catalyzed
Hydrogen radical

ABSTRACT

Acid mine drainage (AMD) contains a large amount of ferrous iron and the recovery of iron oxides from the AMD has been of extensive research interest. Here we report a novel air-cathode fuel cell strategy to in-situ utilize ferrous iron in the AMD for the fabrication of heterogeneous electro-Fenton catalysts. Three types of nano-structured iron oxide/graphite felt (GF) composites, including FeOOH/GF, Fe_2O_3/GF and Fe_3O_4/GF, were fabricated from a synthetic AMD and their catalytic activities towards the electro-Fenton reaction were evaluated at neutral pH with Rhodamine B (RhB) as a probe pollutant. The electro-Fenton system with GF cathode only removed 30 ± 1.4% of RhB after 120 min of reaction. In comparison, RhB removal efficiencies were significantly improved to 62.5 ± 2.0%, 95.4 ± 0.9% and 95.6 ± 0.7% when the FeOOH/GF, Fe_2O_3/GF and Fe_3O_4/GF composites were used as the cathodes, respectively. Among the three types of composites, the Fe_3O_4/GF exhibited the highest electro-Fenton catalytic activity whereas the lowest activity was observed for the FeOOH/GF. The decomposition of H_2O_2 on the iron oxides followed a completely surface-catalyzed mechanism in which the iron oxides maintained their structures without leaching of iron species. The air-cathode fuel cell technology has a potential for iron recovery from the AMD, and provides an effective way for fabricating heterogeneous electro-Fenton catalyst with high catalytic activity and good stability.

1. Introduction

Mining industry produces a large amount of acid mine drainage (AMD) which is characterized as a high acidity effluent containing various dissolved metals and sulfate. As one of the most abundant metals in the AMD, the ferrous iron can cause pollution of natural water and should be removed from the AMD before it is discharged into the environment. The AMD is conventionally deferrized via processes involving alkaline neutralization and air oxidation, producing a chemical sludge containing a mixture of iron oxides such as hematite (Fe_2O_3), magnetite (Fe_3O_4) and geothite (FeOOH) [1,2]. The recovery of iron oxides from AMD residues has been of extensive research interest in order to limit the AMD sludge discharge and offset the cost of AMD treatment [1–3]. However, the complex operational requirements related to the separation of iron oxides make such an iron recovery behavior economically expensive and at poor efficiency.

An alternative approach based on the air-cathode fuel cell has been proposed to selectively treat the ferrous iron in the AMD [4–6]. In such a device, ferrous iron is spontaneously oxidized to form ferric hydroxide at the carbon anode and oxygen in the air is reduced to water at the cathode. Electricity is concomitantly generated during the process, and the produced ferric hydroxide can be transformed to FeOOH upon drying. The primary advantage of the fuel cell approach is it realizes simultaneous recovery of FeOOH and electricity from the AMD under ambient condition [4,5]. However, this approach suffers from difficulties in the collection of iron oxides. The ferric hydroxide produced at the anode may precipitate or be absorbed on the surface of carbon electrode and form iron layers which are hard to be separated [6]. As a result, the iron recovery efficiency is significantly reduced due to the loss of iron oxides on the carbon electrode.

In order to improve the iron recovery efficiency of the fuel cell, here we propose the iron oxides attached to the carbon electrode can be recovered together with the carbon in the form of iron oxide/carbon composite. Carbon supported iron compounds have been widely used in many areas, especially as the catalysts in heterogeneous electro-Fenton processes [7]. The Fenton

* Corresponding author. Fax: +86 551 2901450.
E-mail address: sunmin81@mail.ustc.edu.cn (M. Sun).

http://dx.doi.org/10.1016/j.apcatb.2014.09.077
0926-3373/

reaction is well known for its effectiveness in treating recalcitrant organic pollutants, based on the generation of highly reactive hydrogen radicals from the reaction of ferrous ion (Fe^{2+}) with hydrogen peroxide (H_2O_2) [8]. However, the homogeneous Fenton process has encountered some limitations such as the acidic pH requirement, the self-decomposition of H_2O_2, and the loss of Fe^{2+} into iron sludge [9]. To overcome these drawbacks, heterogeneous electro-Fenton process is developed in which H_2O_2 is continuously supplied by the cathodic reduction of oxygen (O_2) and solid iron compounds (usually iron oxides) serve as the catalysts instead of Fe^{2+} [10,11]. As depicted by Eqs. (1)–(7), a typical heterogeneous electro-Fenton process involves the electro-reduction of O_2 to H_2O_2, the production of hydrogen radicals from H_2O_2 and the oxidation of organic pollutants by hydrogen radicals. The great interest in heterogeneous electro-Fenton process arises from the satisfactory reusability of solid iron catalysts as well as the high conversion efficiency from H_2O_2 to hydrogen radicals [9,10,12].

$$O_2 + 2H_2O + 2e^- \rightarrow H_2O_2 + 2OH^- \quad (1)$$

$$Fe(III) + e^- \rightarrow Fe(II) \quad (2)$$

$$H_2O_2 + Fe(II) \rightarrow Fe(III) + HO\bullet \quad (3)$$

$$H_2O_2 + Fe(III) \rightarrow Fe(II) + HO_2\bullet + H^+ \quad (4)$$

$$HO^\bullet + H_2O_2 \rightarrow HO_2\bullet + H_2O \quad (5)$$

$$HO\bullet + organiccontaminant \rightarrow degradationproducts \quad (6)$$

$$HO_2\bullet + organiccontaminant \rightarrow degradationproducts \quad (7)$$

Therefore, in the present work we report a facile and controllable air-cathode fuel cell strategy to in-situ fabricate heterogeneous electro-Fenton catalyst from a synthetic AMD. Graphite felt (GF) was selected as the supporting material of iron oxides due to its high surface area, good electrochemical stability and high electroconductivity. GF supported iron oxides, including FeOOH/GF, Fe_2O_3/GF and Fe_3O_4/GF, were obtained from the synthetic AMD by using the fuel cell strategy. The catalytic activities of these iron oxide/GF composites towards electro-Fenton reaction were evaluated at neutral pH with Rhodamine B (RhB) as a probe pollutant. The catalytic mechanisms involved in the heterogeneous electro-Fenton process were investigated by characterizing the surface structures of iron oxides and clarifying the roles of free radicals in such a process.

2. Experimental

2.1. Preparation of the iron oxide/GF composites

The iron oxide/GF composites were prepared by loading iron oxides on the GF in an air-cathode fuel cell. The single-chamber glass-made fuel cell architecture was employed with an anodic volume of 175 mL (Fig. 1) [6]. A $3 \times 3\ cm^2$ GF (2 mm in thickness) was located in the chamber as the anode. The cathode was a $2 \times 2\ cm^2$ carbon paper (090S, wet-proofed, Toray Industries Inc., Japan) with a 0.05 mg cm^{-2} platinum catalyst coating on one side. The coated side of the cathode was positioned facing the cation exchange membrane (GEFC-10 N, GEFC Co., China), and the uncoated side was directly exposed to air. Titanium wires (1 mm in diameter) were used to connect the anode and cathode.

A synthetic AMD composed of 40 mM $FeSO_4$, 200 mM NaCl and 50 mM $NaHCO_3$ was used as the anode electrolyte. The anodic chamber was firstly filled with 150 mL of solution that contained NaCl and $NaHCO_3$ and sparged with a mixture of nitrogen (N_2) and carbon dioxide (CO_2) for 30 min to remove dissolved O_2. The $FeSO_4 \cdot 7H_2O$ was then added to the anodic chamber in an anaerobic glove box and the pH was adjusted to 7.0 with HCl under continuous

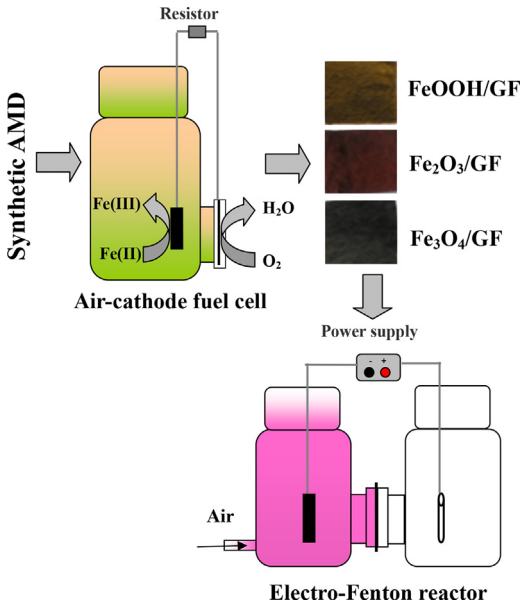

Fig. 1. Schematic diagram for the fabrication of iron oxide/GF composites and their applications in electro-Fenton reaction.

CO_2 sparging. The circuit of fuel cell was left open until a constant open circuit voltage was obtained, and then was connected with a 1000 Ω resistor. A data acquisition system (USB2801, ATD Co., China) was used to monitor the voltage across the 1000 Ω resistor. When the voltage dropped below 1 mV the anode electrode was removed and rinsed with distilled water. The FeOOH/GF composite was prepared by drying the electrode at 40 °C for 24 h. Next, the FeOOH/GF was thermally treated at 300 °C for 1 h in air to obtain the Fe_2O_3/GF composite, or was calcined at 700 °C for 1 h in N_2 to obtain the Fe_3O_4/GF composite.

2.2. Characterization of the iron oxide/GF composites

Iron contents in the iron oxide/GF composites were determined by thermogravimetry (TG) on a TGA DT-50 apparatus (Sahimadzu Corporation, Japan). The TG was performed from room temperature to 1000 °C at a heating rate of 10 °C min^{-1} under air atmosphere. The microscopic images of the composites were obtained using a Sirion 200 scanning electron microscope (SEM) (FEI Co., Netherlands). The crystalline phases of composites were identified by X-ray diffractogram (XRD) using a Bruker D8 advance-X-ray diffractometer equipped with graphite-monochromated Cu Kα radiation (λ = 1.54178 Å). Valence states of iron in the composites were determined using X-ray photoelectron spectroscopy (XPS) on an ESCALAB 250 spectrometer (Thermo, USA) equipped with a monochromatic Mg Kα X-ray source (1253.6 eV). The C1s electron binding energy corresponding to graphitic carbon was set at 284.6 eV and used as a reference to position the other peaks in the XPS spectrum. A nonlinear, Shirley-type baseline and an iterative least-squares fitting algorithm with a Gaussian-Lorentzian sum function were used to deconvolve the XPS peaks. Functional groups in the iron oxides were analyzed by infrared spectrum (IR) on a KBr dist with a VERTEX 70 Fourier transform infrared spectroscopy (Bruker Co., Germany). The composites were cut into $5 \times 5\ mm^2$ pieces for the SEM and XRD analyses, and were ground into powders for the TG, XPS and IR analyses.

Redox activities of the iron oxide/GF composites were evaluated by cyclic voltammetry (CV) on a CHI 660D electrochemical workstation (CH Instruments Inc., USA). The composites ($3 \times 3\ cm^2$) were

used as the working electrodes, Pt was the counter electrode and saturated calomel electrode (SCE) was the reference. The CV was scanned between 0.0 and 2.3 V at 0.1 V s^{-1}, with an initial scanning set at 0.0 V from low to high potential, next followed by a reversed one. The electrolyte solution was 50 mM Na_2SO_4 which was purged with N_2 for 30 min prior to CV scanning, and the N_2 atmosphere was maintained over the solution throughout the measurement.

2.3. Electro-Fenton degradation of RhB

The electro-Fenton degradation of RhB was carried out in a two-chamber glass-made reactor with the anode and cathode each in a 175 mL cylindrical chamber separated by a cation exchange membrane (GEFC-10 N, GEFC Co., China) (Fig. 1). A 5 cm graphite rod (Φ = 5 mm) was used as the anode and the prepared iron oxide/GF composites were the cathodes. The 50 mM Na_2SO_4 was used as the electrolyte in both the anodic and cathodic chambers, while the cathodic electrolyte contained 5.0 mg L^{-1} of RhB at a pH of 6.8. Electrolysis experiment was performed by applying a constant voltage of 2.0 V from a PS3003 DC power supply (QJE Co., China). Air was bubbled at a rate of 1.5 L min^{-1} from the bottom of the cathodic chamber throughout the electrolysis to ensure the cathode electrolyte was saturated with O_2. Samples were taken periodically from the cathodic chamber to measure concentrations of RhB, H_2O_2 and hydroxyl (HO•) radical.

2.4. Chemical analysis

The concentration of RhB was determined by colorimetry at λ = 553 nm. The concentration of Fe^{2+} was measured using the modified phenanthroline method and concentration of ferric ion (Fe^{3+}) was determined after being reduced to Fe^{2+} by ascorbic acid [13]. The concentration of H_2O_2 was determined by iodide method [14]. The HO• radical produced during the electro-Fenton process was quantified spectrophotometrically at λ = 440 nm with *p*-nitrosodimethylaniline as an indicator [15].

3. Results

3.1. Characterizing the structures and morphologies of iron oxide/GF composites

Fig. 2 shows the XRD patterns of as-prepared iron oxide/GF composites. One typical peak assigned to the 002 facet of GF (JCPDS 29-071341-1487) is observed at the 2θ value of 25.0° on the patterns of all the three samples. The FeOOH/GF composite contains only one pure orthorhombic phase of α-FeOOH with cell constants of *a* = 4.608 Å, *b* = 9.956 Å and *c* = 3.022 Å, evidenced by the diffraction peaks located at 2θ values of 21°, 33°, 34°, 35°, 36°, 39°, 41°, 53°, 59° and 61° (JCPDS 29-0713) on the XPS pattern. By thermal treatment at 300 °C for 1 h in air, α-FeOOH was completely converted to the hexagonal α-Fe_2O_3 phase with cell constants of α = 5.035 Å and *c* = 13.747 Å, which displays peaks at 2θ values of 24°, 33°, 36°, 41°, 53°, 57°, 62° and 64° (JCPDS 33-0664). As the α-FeOOH was annealed at 700 °C for 1 h in N_2, it transformed to the face-centered-cubic Fe_3O_4 with diffraction peaks located at 2θ values of 30°, 35°, 37°, 43°, 53°, 57° and 63° (JCPDS 19-0629).

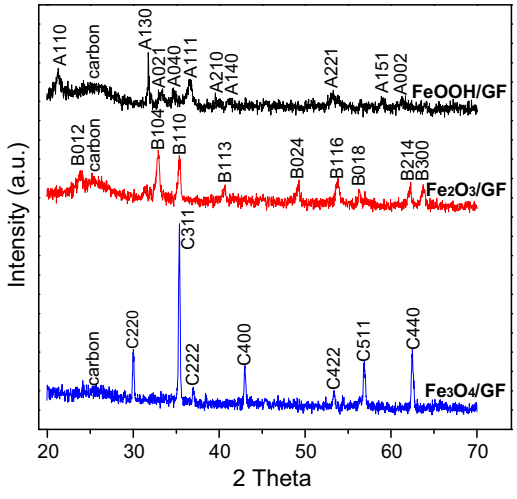

Fig. 2. XRD patterns of the prepared iron oxides/GF composites.

The morphologies of iron oxide/GF composites were observed by SEM images. As shown in Fig. 3, the carbon surface is covered with layers of nano-sized iron oxides. The FeOOH is spread on the carbon surface as clusters of nanospindles with diameters from 50 to 150 nm, whereas the Fe_2O_3 displays flower-like structure composed of interconnected nanoflakes with a thickness of about 30 nm. The Fe_3O_4 particles are presented as monodispersed nanocubes with edge lengths in the range of tens to hundreds of nanometers.

According the TG analysis (See Supplementary Material), iron contents in the FeOOH/CF, Fe_2O_3/CF and Fe_3O_4/CF composites were calculated to be 18.5 wt%, 18.9 wt% and 17.7 wt%, respectively, which were higher than the values reported for the iron oxide/carbon composites even used in heterogeneous electro-Fenton systems [11,16].

CV was performed on the iron oxide/GF composites to investigate their redox properties as the electro-Fenton catalysts (Fig. 4). Bare GF shows no peaks on the cyclic voltammogram, whereas one couple of redox peaks attributed to the transformations between Fe(II) and Fe(III) appear on the voltammograms of the composites. Such redox peaks are very weak for the FeOOH/GF, with anodic and cathodic peaks located at ca. 0.534 and 0.846 V, respectively. Significantly enhanced peak intensities are observed on the voltammograms of the Fe_2O_3/GF and Fe_3O_4/GF, which suggests stronger redox activities of the two composites compared to the FeOOH/GF. Since the redox activity is essential for the catalyst to perform electron transfer during electro-Fenton reaction, it is anticipated the prepared iron oxide/GF composites have great potentials to be used as the electro-Fenton catalysts.

3.2. Comparing the RhB removal efficiencies in electro-Fenton systems with different iron oxides/GF composite cathodes

Fig. 5 shows the removal of RhB with respect to time in electro-Fenton systems with different iron oxide/GF composites as the cathodes. Bare GF demonstrated very limited electro-Fenton catalytic activity, given the RhB removal efficiency of only 30 ± 1.4% after 120 min of reaction. The RhB removal efficiencies achieved as high as 62.5 ± 2.0%, 95.4 ± 0.9% and 95.6 ± 0.7% in the systems with FeOOH/GF, Fe_2O_3/GF and Fe_3O_4/GF cathodes, respectively, implying enhanced electro-Fenton catalytic activities of the prepared composites. Among the three types of composites, the Fe_3O_4/GF showed the highest catalytic activity while the lowest activity was observed on the FeOOH/GF. The electro-Fenton system obtained 77.4 ± 1.4% of RhB removal efficiency within 30 min by using the Fe_3O_4/GF cathode. Such a value decreased to 69.5 ± 3.8% using the Fe_2O_3/GF cathode and further to 50.4 ± 1.9% using the FeOOH/GF one. Such a result was in agreement with the redox activities of the corresponding composites observed in the CV analysis.

RhB adsorption experiments were performed to evaluate if the adsorption played a role in the RhB removal. The RhB adsorption efficiencies were generally less than 10% on the iron oxide/GF

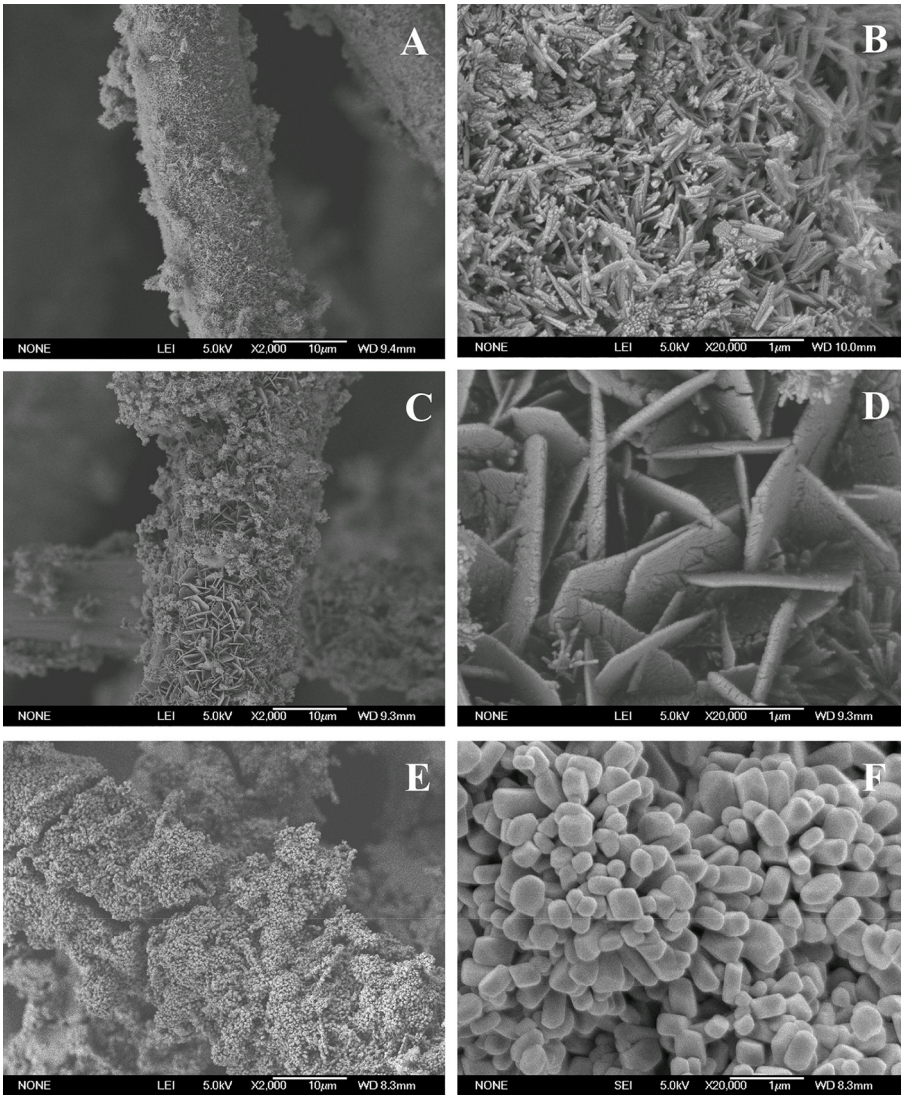

Fig. 3. SEM images of the prepared (A) and (B): FeOOH/GF; (C) and (D): Fe_2O_3/GF; and (E) and (F): Fe_3O_4/GF composites.

composites, suggesting the poor RhB adsorption capacities of these materials. Therefore, the high RhB removal efficiencies in the electro-Fenton systems were attributed to the degradation of RhB rather than the adsorption of RhB on the cathodes.

3.3. Elucidating mechanisms involved in the electro-Fenton process

Fig. 6 shows concentration profiles of H_2O_2 and HO• radicals during the electro-Fenton process in the absence of RhB. The concentration of H_2O_2 firstly increased with reaction time and

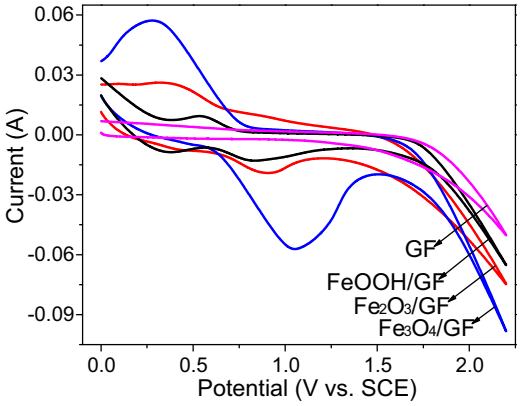

Fig. 4. Cyclic voltammograms of GF and iron oxides/GF composites in 50 mM Na_2SO_4 solution.

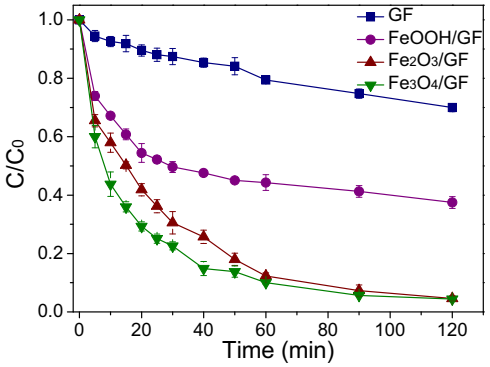

Fig. 5. RhB removals in electro-Fenton systems with GF and iron oxide/GF composites as the cathodes.

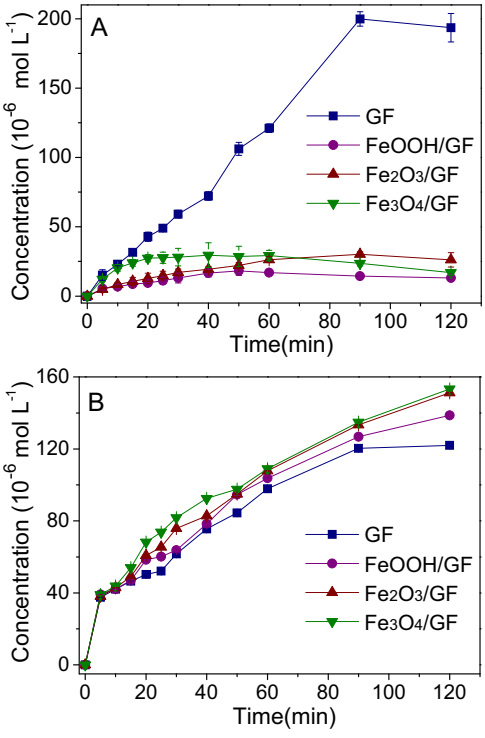

Fig. 6. Time course evolutions of (A) H_2O_2 and (B) HO• concentrations in electro-Fenton systems with GF and iron oxide/GF composites as the cathodes in the absence of RhB.

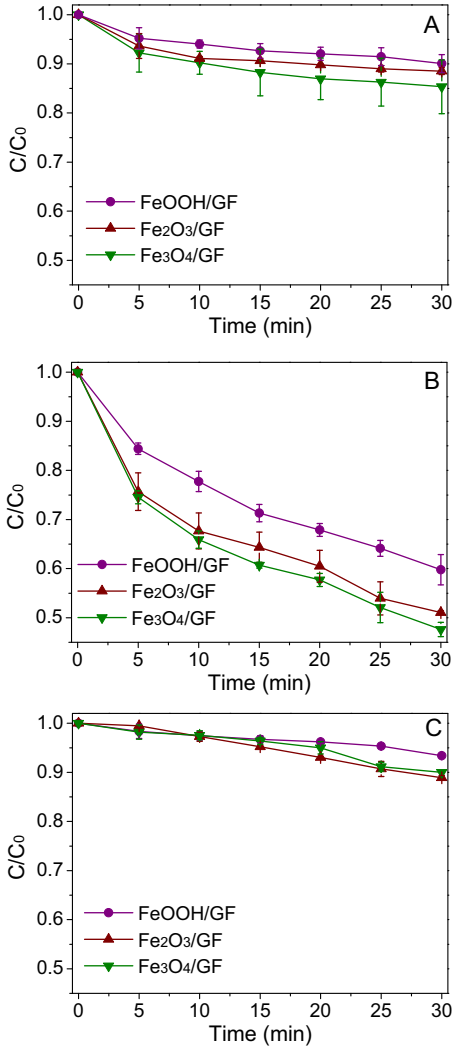

Fig. 7. RhB removals in electro-Fenton systems added with (A) isopropanol; (B) benzoquinone; and (C) isopropanol and benzoquinone.

then slightly decreased, while concentration of HO• exhibited a rising tendency throughout the whole process. Since the H_2O_2 electro-generated at the cathode could be decomposed to hydrogen radicals (Eqs. (3)–(5)), the amount of H_2O_2 accumulated in bulk solution was decided by both the production and decomposition rates of H_2O_2. At the initial stage of reaction, the increase of H_2O_2 concentration implied a higher H_2O_2 production rate than its decomposition rate. And the decreased concentration of H_2O_2 at the latter stage should be attributed to the slower H_2O_2 production compared to its consumption.

As shown in Fig. 6, concentrations of H_2O_2 in the systems with the iron oxide/GF composite cathodes were lower than that with the GF cathode, whereas concentrations of HO• radical generated on the composites were generally higher. This fact suggests the decomposition of H_2O_2 to the HO• radical can be effectively accelerated by the catalysis of iron oxides. What should be noted is that the highest HO• concentration was obtained in the system with Fe_3O_4/GF cathode and the lowest was in that with FeOOH/GF cathode among the tree types of composites. Such an observation was in good accordance with the result that RhB was removed the fastest on the Fe_3O_4/GF cathode whereas the slowest on the FeOOH/GF one.

Besides the HO• radical, the peroxide (HO_2•) radical may also be generated from the decomposition of H_2O_2, which is presented in the form of the conjugate base as superoxide anion ($•O_2^-$) [17]. Herein, the roles of HO• and $•O_2^-$ radicals playing in the RhB degradation were examined by using isopropanol and benzoquinone as the scavengers of HO• and $•O_2^-$ radicals, respectively [10]. The concentration of added radical scavenger was 1000 times greater than the concentration of RhB to ensure the radicals were totally quenched. Within the initial 30 min, RhB degradations on the FeOOH/GF, Fe_2O_3/GF and Fe_3O_4/GF cathodes were significantly inhibited by 77.2%, 78.9% and 80.4% after isopropanol addition (Fig. 7A). Such an inhibitory effect was much weaker when benzoquinone was added, with RhB removal efficiencies reduced by 20.1%, 29.5% and 32.3% for the three cathodes, respectively (Fig. 7B). These results suggest both the HO• and $•O_2^-$ radicals were responsible for the RhB degradation, while the RhB degradation efficiency relied mainly on the HO• and to less extent on the $•O_2^-$. It is noteworthy that more than 6% of RhB was removed after 30 min in the systems with both the isopropanol and benzoquinone (Fig. 7C), whereas the adsorption experiment revealed RhB adsorption efficiencies on these composites were only 2.5% for the same time duration. Therefore, there should be non-radical mechanism involved in the RhB degradation, although its contribution was very small.

3.4. Evaluating the stabilities of iron oxide/GF composites in electro-Fenton process

The iron oxide/GF composites exhibited good reusabilities as the cathodes of electro-Fenton system, evidenced by the well maintained RhB removal efficiencies in eight successive batches (Fig. 8). Furthermore, neither Fe^{2+} nor Fe^{3+} were detected during the recycling operation, indicating a completely surface-catalyzed electro-Fenton mechanism on the composites.

Valence states of iron in the composites before and after eight successive batches were analyzed by deconvoluting the XPS Fe2p spectra. As shown in Fig. 9, the Fe2p levels are split into $2p_{3/2}$ and

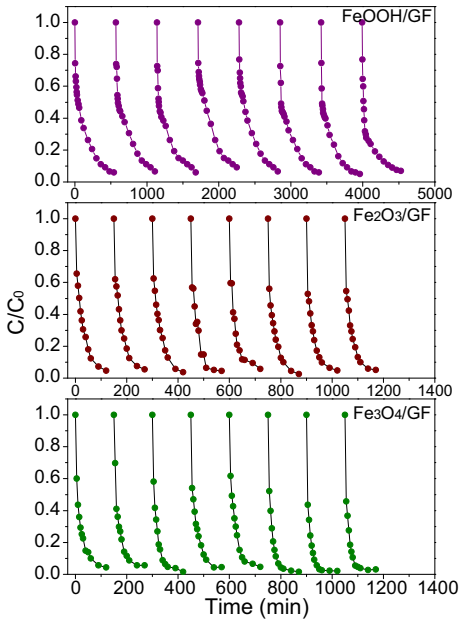

Fig. 8. RhB removals in eight successive cycles with different iron oxide/GF composite cathodes.

$2p_{1/2}$ doublets due to the spin-orbit coupling. For the FeOOH/GF, the peaks of $Fe2p_{3/2}$ and $Fe2p_{1/2}$ are observed at 712.2 and 725.9 eV, respectively, accompanied by a charge transfer satellite peak of $Fe2p_{3/2}$ located at 720.0 eV. The XPS spectrum of Fe_2O_3/GF also shows a satellite peak at 720.0 eV, other than the $Fe2p_{3/2}$ peak at 711.6 eV and $Fe2p_{1/2}$ peak at 725.3 eV. The satellite peak is approximately 8 eV higher than the $Fe2p_{3/2}$ main peak on the spectra of both the FeOOH/GF and Fe_2O_3/GF, suggesting the absence of Fe(II) in the two composites [18]. Such a satellite structure disappears from the XPS spectrum of Fe_3O_4/GF, as it was reported for Fe_3O_4 in the literature [19], leaving only the $Fe2p_{3/2}$ and $Fe2p_{1/2}$ main

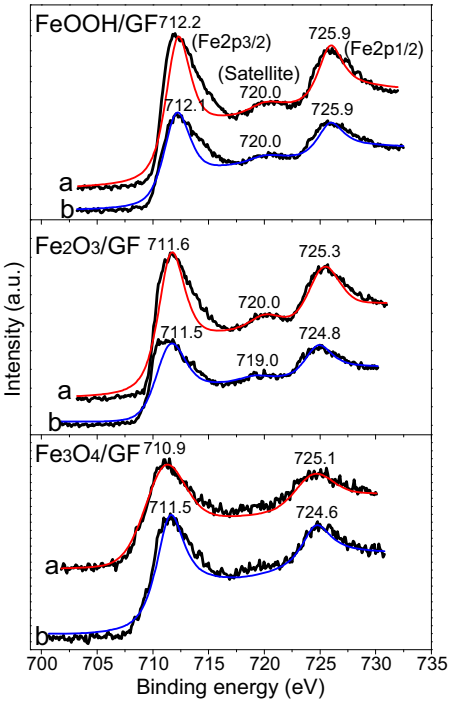

Fig. 9. Fe 2p XPS spectra of the iron oxides/GF composite cathodes (a) before and (b) after eight successive cycles.

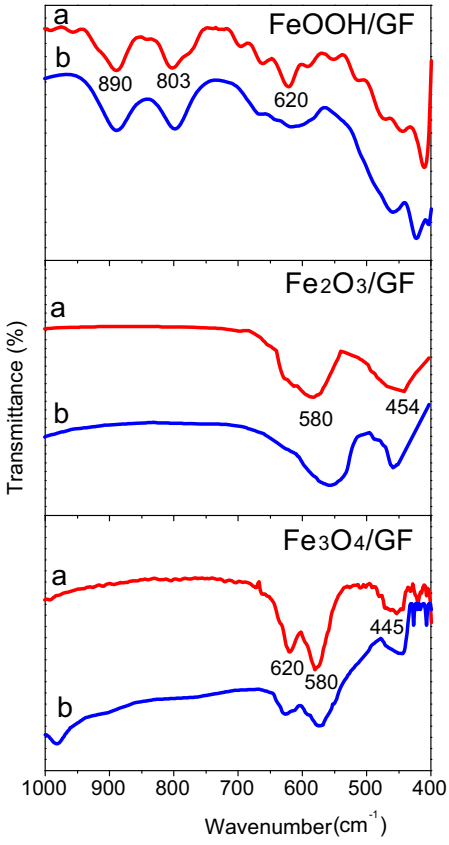

Fig. 10. FT-IR spectra of the iron oxides/GF composite cathodes (a) before and (b) after eight successive cycles.

peaks at 710.9 and 725.1 eV, respectively. Since the Fe 2p peaks of the composites undergoing recycling operation remain the same as those of the fresh ones, it is proposed the valence states of iron in these composites can be recovered after electro-Fenton reaction.

FT-IR spectra of the fresh and used composites were compared to further evaluate their stabilities in the electro-Fenton process (Fig. 10). Two typical bands which are assigned to Fe-O-H bending vibrations are observed at 890 and 803 cm^{-1} on the IR spectra of FeOOH/GF, and the adsorption band at 620 cm^{-1} is attributed to Fe—O stretching vibration in the FeOOH [20,21]. The Fe—O adsorption bands are also found on the spectra of Fe_2O_3/GF and Fe_3O_4/GF composites, which appear at 580 and 450 cm^{-1} for the Fe_2O_3 and at 620, 580 and 445 cm^{-1} for the Fe_3O_4, respectively [22,23]. The characteristic bands of each iron oxide are well maintained and new bands due to other iron oxides are not detected on the spectra of the used composites, suggesting the structures of iron oxides were not changed by the electro-Fenton reaction. Moreover, the XRD analysis indicates the crystalline phases of iron oxides were also retained after reaction (Fig. S2, See Supplementary Material). Therefore, it is concluded the iron oxides in the composites are able to keep their compositions and structures in the electro-Fenton process.

4. Discussion

4.1. Prospective of the air-cathode fuel cell technology

In this work, GF supported iron oxides with favorable electro-Fenton catalytic activities are fabricated from a synthetic AMD by using an air-cathode fuel cell. In comparison to traditional AMD treatments, a major advantage of the fuel cell strategy is it realizes the in-situ utilization of iron wastes in the AMD. Besides, this

strategy has the merit of controllability and flexibility that carbon supported iron oxides with varied compositions and structures can be obtained via regulating the calcinating condition. Moreover, the fact that such a strategy does not involve any organic solvents makes it environmentally and economically preferable to other fabrication methods of iron oxides.

Here we provide a very basic process to demonstrate the feasibility of the fuel cell technology in the fabrication of heterogeneous electro-Fenton catalysts from the AMD. Practical applications of this technology will require further developments of process, including the application of high surface area carbon to enhance the iron loading, the manipulation of fuel cell as well as subsequent calcination process to modify the structure of iron oxide for improved catalytic activity, and the optimization of parameters of electro-Fenton process to achieve more effective and economic pollutant removal.

4.2. Relationship between the surface structure and catalytic activity of iron oxide

The iron oxide/GF composites prepared in this work exhibit promising performances in catalyzing the electro-Fenton reaction. Iron oxides themselves can activate H_2O_2 and produce free radicals [24], and the nano structure of as-prepared iron oxides enhances such activation abilities because of their large specific surface where catalytically active sites are exposed [25]. The Fe_3O_4/GF composite shows quite higher catalytic activity than the Fe_2O_3/GF and FeOOH/GF composites. Given the fact that the iron loadings in these composites are very similar, this difference on the catalytic activity should be attributed to the different structures of the iron oxides. As regards mineral type, Fe(III) oxides are catalytically less active than their Fe(II) counterparts [26]. Unlike FeOOH or Fe_2O_3 whose catalytic activity should be triggered by converting Fe(III) to Fe(II), the Fe_3O_4 contains Fe(II) which directly acts as an electron donor to initiate the Fenton reaction. Moreover, the octahedral site in the Fe_3O_4 structure accommodates both the Fe (II) and Fe (III) and thus facilitates the inter-conversion between Fe(II) and Fe(III) [27].

Heterogeneous electro-Fenton process with solid iron catalysts has been of extensive research interest in order to overcome problems related to the iron sludge and iron loss in homogeneous electro-Fenton process. However, in most heterogeneous electro-Fenton systems the solid iron catalysts act as self-regulators of iron supply which release Fe^{2+} to the bulk to react with electro-generated H_2O_2 [28–31]. These systems are virtually controlled by the homogeneous catalysis mechanism, and the activities of catalysts deteriorate with repeated use because of the leaching of Fe^{2+} from the catalysts to aqueous phase. Quite different from above, the heterogeneous electro-Fenton process presented in this work is totally catalyzed by the solid iron oxides without participation of soluble iron species. The iron oxides are able to maintain their structures after electro-Fenton reaction, which assures their activities in long-term of recycling utilization.

4.3. Roles of free radicals in the degradation of RhB

The catalytic mechanism through which H_2O_2 is activated by iron oxide is an important issue for the heterogeneous electro-Fenton process. Most investigators approve the activation of H_2O_2 follows a radical pathway which generates HO• and HO_2• radicals to oxidize pollutants [32]. However, others argue the radical mechanism cannot appropriately describe the reaction of H_2O_2 over the solid iron oxide [17]. Alternatively, they suggest the H_2O_2 may be activated through a non-radical mechanism that related to the direct electron transfer between H_2O_2 and the pollutant on the surface of iron oxide [33,34]. In this work, we find both the radical and non-radical mechanisms are involved in the RhB degradation by H_2O_2 on the surface of iron oxide/GF composites, with the radical mechanism responsible for the most of RhB degradation while the non-radical mechanism only playing a minor role.

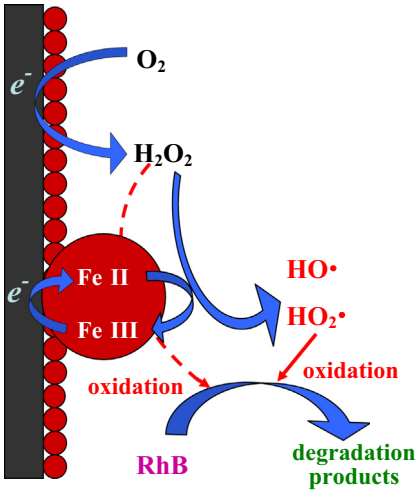

Fig. 11. Schematic illustration of heterogeneous electro-Fenton mechanism on the iron oxide/GF composite cathodes.

Both the HO• and HO_2• radicals can be generated from the decomposition of H_2O_2, whereas the HO• radical exhibits significantly higher oxidation power than the HO_2• radical [32]. In order to achieve an effective pollutant removal it is necessary to promote the generation of HO• while restrain the generation of HO_2• radical. However, the excessive H_2O_2 in traditional Fenton process facilitates the $HO_2^{\bullet}$ production via Eq. (5), thereby leading to a low pollutant removal efficiency and a waste of H_2O_2 [35]. Such a problem has been controlled in the electro-Fenton process. Since the H_2O_2 generated at the cathode is rapidly decomposed without accumulation, the highly reactive $HO^{\bullet}$ radical dominates the electro-Fenton process which assures the treatment at high efficiency.

On the basis of the obtained information, a possible surface-catalyzed pathway for the RhB degradation in the heterogeneous electro-Fenton process is proposed and depicted in Fig. 11. Firstly, O_2 is absorbed on the cathode and electro-reduced to H_2O_2, meanwhile the Fe(III) in iron oxide being reduced to the Fe(II) state. Next, the H_2O_2 decomposes at the Fe(II) site to generate hydrogen radicals such as HO• and HO_2• which then oxidize and degrade RhB. At the same time the Fe(II) is oxidized back to the Fe(III) state. In this way, the iron oxide is in-situ recycled. The H_2O_2 may also oxidize RhB via a direct electron transfer over the surface of iron oxide.

5. Conclusions

Nano-structured iron oxide/GF composites with favorable electro-Fenton catalytic activities were fabricated from a synthetic AMD by using the air-cathode fuel cell. Such a fuel cell strategy demonstrated the advantage of controllability and flexibility that carbon supported iron oxides, including FeOOH/GF, Fe_2O_3/GF and Fe_3O_4/GF, could be obtained via regulating the calcinating condition. Experiments on the RhB degradation suggested a higher electro-Fenton catalytic activity of Fe_3O_4/GF than the Fe_2O_3/GF and FeOOH/GF composites, which was attributed to the presences of Fe(II) and octahedral site in the Fe_3O_4 structure. Both the HO• and HO_2• radicals were generated from the decomposition of H_2O_2, while the HO• radicals were responsible for the majority of RhB degradation. The heterogeneous electro-Fenton reaction occurring on the iron oxide/GF composites at neutral pH was suggested to be

completely surface-catalyzed without participation of soluble iron species. The iron oxides maintained their structures in the electro-Fenton process, therefore exhibiting good stabilities in the recycling utilization.

Acknowledgements

The authors wish to thank the NSFC (51478157, 51378166) and the Program for New Century Excellent Talents in University (NCET-13-0767) for the financial support of this work.

Appendix A. Supplementary data

Supplementary data associated with this article can be found, in the online version, at http://dx.doi.org/10.1016/j.apcatb.2014.09.077.

References

[1] S.L.F. Andersen, R.G. Flores, V.S. Madeira, H.J. Jose, R.F.P.M. Moreira, Ind. Eng. Chem. Res. 51 (2012) 767–774.
[2] R.A. Silva, C.D. Castro, E.M. Viganico, C.O. Petter, I.A.H. Schneider, Miner. Eng. 29 (2012) 22–27.
[3] X.C. Wei, R.C. Viadero, K.M. Buzby, Environ. Eng. Sci. 22 (2005) 745–755.
[4] S. Cheng, B.A. Dempsey, B.E. Logan, Environ. Sci. Technol. 41 (2007) 8149–8153.
[5] S. Cheng, J.H. Jang, B.A. Dempsey, B.E. Logan, Water Res. 45 (2011) 303–307.
[6] M. Sun, W. Song, L.F. Zhai, Z.H. Tong, J. Power Sources 248 (2014) 6–14.
[7] E.G. Garrido-Ramirez, B.K.G. Theng, M.L. Mora, Appl. Clay Sci. 47 (2010) 182–192.
[8] J.J. Pignatello, E. Oliveros, A. MacKay, Crit. Rev. Environ. Sci. Technol. 36 (2006) 1–84.
[9] A. Ozcan, Y. Sahin, M.A. Oturan, Water Res. 47 (2013) 1470–1479.
[10] H. Zhao, Y. Wang, Y. Wang, T. Cao, G.E. Zhao, Appl. Catal. B: Environ. 125 (2012) 120–127.
[11] Y. Wang, H. Zhao, S. Chai, Y. Wang, G. Zhao, D. Li, Chem. Eng. J. 223 (2013) 524–535.
[12] H.H. Huang, M.C. Lu, J.N. Chen, Water Res. 35 (2001) 2291–2299.
[13] L. Herrera, P. Ruiz, J.C. Aguillon, A. Fehrmann, J. Chem. Technol. Biotechnol. 44 (1989) 171–181.
[14] N.V. Klassen, D. Marchington, H.C.E. McGowan, Anal. Chem. 66 (1994) 2921–2925.
[15] Q. Xue, M. Li, K. Shimizu, M. Utsumi, Z. Zhang, C. Feng, Y. Gao, N. Sugiura, Desalination 265 (2011) 135–139.
[16] S. Liu, X.R. Zhao, H.Y. Sun, R.P. Li, Y.F. Fang, Y.P. Huang, Chem. Eng. J. 231 (2013) 441–448.
[17] S.S. Lin, M.D. Gurol, Environ. Sci. Technol. 32 (1998) 1417–1423.
[18] L. Zeng, W. Ren, J. Zheng, A. Wu, P. Cui, Appl. Surf. Sci. 258 (2012) 2570–2575.
[19] G. Xie, P. Xi, H. Liu, F. Chen, L. Huang, Y. Shi, F. Hou, Z. Zeng, C. Shao, J. Wang, J. Mater. Chem. 22 (2012) 1033–1039.
[20] S. Bashir, R.W. McCabe, C. Boxall, M.S. Leaver, D. Mobbs, J. Nanopart. Res. 11 (2009) 701–706.
[21] R. Zamiri, H.A. Ahangar, A. Zakaria, G. Zamiri, H.R. Bahari, G.P.C. Drummen, J. Nanopart. Res. 16 (2014) 2333.
[22] F. Cheng, K. Huang, S. Liu, J. Liu, R. Deng, Electrochim. Acta 56 (2011) 5593–5598.
[23] H. Firouzabadi, N. Iranpoor, M. Gholinejad, S. Akbari, N. Jeddi, RSC Adv. 4 (2014) 17060–17070.
[24] F. Lucking, H. Koser, M. Jank, A. Ritter, Water Res. 32 (1998) 2607–2614.
[25] J. Nurmi, P.G. Tratnyek, V. Sarathy, D.R. Baer, J.E. Amonette, K. Pecher, C. Wang, J.C. Linehan, D.W. Matson, R.L. Penn, M.D. Driessen, Environ. Sci. Technol. 39 (2005) 1221–1230.
[26] W.P. Kwan, B.M. Voelker, Environ. Sci. Technol. 37 (2003) 1150–1158.
[27] R.C.C. Costa, F.C.C. Moura, J.D. Ardisson, J.D. Fabris, R.M. Lago, Appl. Catal. B: Environ. 83 (2008) 131–139.
[28] J. Li, Z. Ai, L. Zhang, J. Hazard. Mater. 164 (2009) 18–25.
[29] G. Zhang, S. Wang, F. Yang, J. Phys. Chem. C 116 (2012) 3623–3634.
[30] E. Rosales, O. Iglesias, M. Pazos, M.A. Sanroman, J. Hazard. Mater. 213–214 (2012) 369–377.
[31] M. Luo, S. Yuan, M. Tong, P. Liao, W. Xie, X. Xu, Water Res. 48 (2014) 190–199.
[32] E. Brillas, I. Sirés, M.A. Oturan, Chem. Rev. 109 (2009) 6570–6631.
[33] A.L. Teel, C.R. Warberg, D.A. Atkinson, R.J. Watts, Water Res. 35 (2001) 977–984.
[34] R. Andreozzi, V. Caprio, R. Marotta, Water Res. 36 (2002) 2761–2768.
[35] F. Duarte, V. Morais, F.J. Maldonado-Hódar, L.M. Madeira, Chem. Eng. J. 232 (2013) 34–41.